The International Journal of
Robotics Research
32(6) 637–649

DOI: 10.1177/0278364913479412
ijr.sagepub.com

Closed-loop control of magnetotactic bacteria

Islam S. M. Khalil[1], Marc P. Pichel[1], Leon Abelmann[2] and Sarthak Misra[1]

Abstract

Realization of point-to-point positioning of a magnetotactic bacterium (MTB) necessitates the application of a relatively large magnetic field gradients to decrease its velocity in the vicinity of a reference position. We investigate an alternative closed-loop control approach to position the MTB. This approach is based on the characterization of the magnetic dipole moment of the MTB and its response to a field with alternating direction. We do not only find agreement between our characterized magnetic dipole moment and previously published results, but also observe that the velocity of the MTB decreases by 37% when a field with alternating direction is applied at 85 Hz. The characterization results allow us to devise a null-space control approach which capitalizes on the redundancy of magnetic-based manipulation systems. This approach is based on two inputs. The first controls the orientation of the MTB, whereas the second generates a field with alternating direction to decrease its velocity. This control is accomplished by the redundancy of our magnetic-based manipulation system which allows for the projection of the second input onto the null-space of the magnetic force-current map of our system. A proportional–derivative control system positions the MTB at an average velocity and region of convergence of 29 $\mu m\ s^{-1}$ and 20 μm, respectively, while our null-space control system achieves an average velocity and region of convergence of 15 $\mu m\ s^{-1}$ and 13 μm, respectively.

Keywords

magnetic, frequency response, dipole moment, redundancy, null space

1. Introduction

Closed-loop control of living microorganisms such as magnetotactic bacteria (MTBs) (Blakemore, 1975) can allow them to reach various hard-to-access regions within the human body in a minimally invasive manner (Martel et al., 2009b; Nelson et al., 2010). The size of the MTBs provides them with a wide range of applications. The smallest capillaries of the human blood circulatory system have diameters which range from 6 to 10 μm (Martel et al., 2004), whereas the average diameter and length of the membrane of the MTB, i.e. *Magnetospirillum magnetotacticum* MS-1, are 0.5 and 5 μm, respectively, as shown in Figure 1.

During the magnetic-based control of such microorganisms, external fields are generated to orient the MTB towards a reference position. The self-propulsion provided by its flagella allows for the navigation towards this reference position. In order to realize *point-to-point* positioning of an MTB, not only do we need to control the direction of the field based on the position tracking error, but we also have to control (decrease) the velocity of the MTB. This control is required due to the self-propulsion of the MTB which does not allow the position tracking error to go to zero. Controlling the velocity of the MTB requires relatively large field gradients to generate a pulling force to overcome the propulsion force generated by the flagella. Although the self-propulsion force has an order of magnitude of 10^{-12} N (Martel et al., 2006), the magnetic dipole moment of the MTB has an order of magnitude which ranges from 10^{-18} to 10^{-16} A m^{-2} (Bahaj et al., 1996). This requires the generation of relatively large field gradients. Such gradients can be provided by modern magnetic resonance imaging systems. Therefore, we investigate an alternative approach to control the motion of an MTB using relatively low magnetic fields and field gradients. This approach is based on characterizing the magnetic dipole moment and

[1]MIRA–Institute for Biomedical Technology and Technical Medicine, University of Twente, The Netherlands
[2]MESA+ Institute for Nanotechnology, University of Twente, The Netherlands

Corresponding author:
Islam S. M. Khalil, Faculty of Electrical Engineering, Mathematics & Computer Science, University of Twente, P.O. Box 217, Carre 3.710 (RAM-EWI), 7500 AE Enschede, The Netherlands.
Email: i.s.m.khalil@utwente.nl

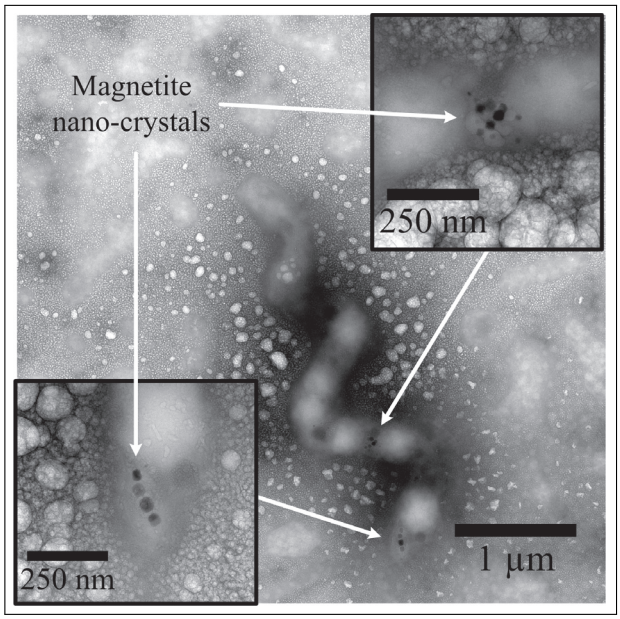

Fig. 1. Scanning/transmission electron microscopy (SEM/TEM) images of the magnetotactic bacterium (MTB), i.e. *Magnetospirillum magnetotacticum* MS-1. The SEM image shows the spiral membrane of the MTB which envelopes chains of magnetite nanocrystals. This membrane has an average diameter and length of 0.5 and 5 μm, respectively. The two insets show TEM images of the magnetite nanocrystals which provide a magnetic dipole moment. An MTB uses this magnetic dipole moment to orient itself along external magnetic field lines.

the response of the MTB to a field with alternating direction, and capitalizes on the redundancy of magnetic-based manipulation systems.

There are relatively a few attempts related to the magnetic-based open-loop control of magnetic microorganisms. Martel and Mohammadi (2010) demonstrated that a swarm of flagellated MTBs, i.e. *Magnetococcus* MC-1, can be used to accurately manipulate micro-components via the thrust force generated by the flagella bundles. It was further shown that *Magnetospirillum gryphiswaldense* MTBs can be used to manipulate a 3 μm bead along a path with an average velocity of 7.5 μm s^{-1} without exerting a propulsion force on either the bacteria or the beads (Martel et al., 2006). A swarm of *Serratia marcescene* was attached to fluorescent beads and chips to provide propulsion, and random motion was observed without applying motion control (Darnton et al., 2004). Motile bacteria of the same strain (*Serratia marcescene*) were integrated with a microstructure and controlled by the self-propulsion and DC electric fields using a vision feedback control system (Sakar et al., 2011). Although the aforementioned work provide novel approaches to control a swarm of magnetotactic microorganisms, *point-to-point* control of a single MTB remains a challenge. Ou et al. (2012) presented a Model Predictive Control system to control the motion of magnetotactic *Tetrahymena pyriformis* based on a discrete-time model. Open-loop control and proportional–derivative (PD) control of an MTB were demonstrated by Khalil et al. (2012c). The open-loop control allowed the MTB to follow different trajectories, while the PD control positioned the MTB within a region of convergence of 10 μm in diameter.

Closed-loop control of an MTB requires the characterization of its magnetic dipole moment. The magnetic dipole moment can be determined by several techniques for motile and non-motile MTBs (Steinberger et al., 1994; Erglis et al., 2007). Transmission electron microscopy (TEM) images can be used to deduce the magnetic dipole moment from the size and number of the magnetosomes that are enveloped inside the membrane of the MTB (Figure 1). A *U-turn* technique was presented to determine the magnetic dipole moment of the MTB by applying magnetic field reversals (Bahaj and James, 1993). The magnetic dipole moment was calculated using the diameter of the *U-turn* trajectory of the MTB.

Pan et al. (2009) showed that the velocity of the bacterial strain *Magnetococcus* MYC-1 decreases by increasing the magnetic field strength. This decrease was attributed to the angular deviation between the axis of the magnetite nanocrystals and the flagellar propulsion axis which causes the helical trajectories taken by the MYC-1 to increase. The helical trajectories of the bacterial strain *magneto-ovoid* MO-1 was modeled using a six-degree-of-freedom dynamic model. This model was verified by comparing the simulated motion with the motion of the bacteria under the influence of magnetic field reversals and rotational magnetic fields (Nogueira and Lins De Barros, 1995; Yang et al., 2012). It has been observed that the velocity of the MTB depends on the rotational and vibrational modes of its flagella. These modes were determined using a super conducting quantum interference device microscope (Chemla et al., 1999). Perturbing these modes could change the velocity of the MTB. This observation requires the investigation of the response of the MTB to a field with alternating direction. Such frequency response is determined by measuring the linear velocity of the MTB at different frequencies of a field with alternating direction. This frequency response can be used to devise a control system that employs the field with alternating direction to perturb the modes of the MTB to change its velocity.

In this work, we present a null-space control system which allows for the *point-to-point* positioning of an MTB. This null-space control system is based on the redundancy of magnetic-based manipulation systems. Magnetic redundancy is utilized to provide an auxiliary control input to perturb the modes of the flagella of the MTB. This auxiliary input along with the main control input achieve accurate positioning of the MTB, as opposed to a PD control system (both control systems are evaluated on the same culture of MTBs). Characteristics of the transient- and steady-state are used to evaluate the performance and accuracy of the PD and null-space control systems. In addition, the proposed null-space control system allows for the positioning of the

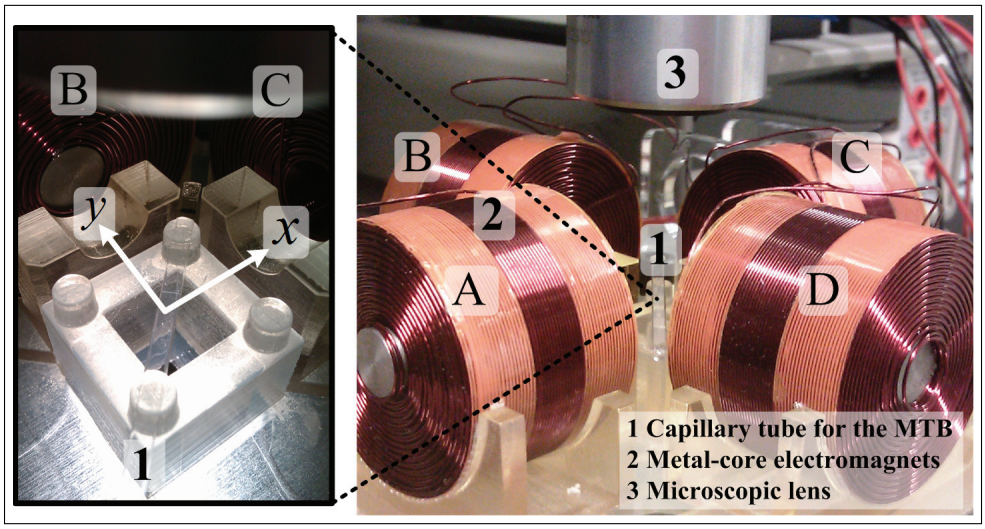

Fig. 2. Magnetic-based manipulation system for the characterization and the closed-loop control of a magnetotactic bacterium (MTB). The system consists of an array of metal-core electromagnets and equipped with a microscopic vision system. The array of electromagnets surrounds a flat capillary tube (VitroTubes 3520-050, VitroCom, Mountain Lakes, USA) which incubates a culture of MTBs, i.e. *M. magnetotacticum* MS-1. The capillary tube has an inner thickness, an inner width and length of 0.2 mm, 2 mm and 50 mm, respectively. The inset shows the capillary tube which incubates the growth medium of the MTBs. The electromagnets are labeled with the letters A, B, C and D (Keuning et al., 2011; Khalil et al., 2012a).

MTB and changing its velocity without pulling by the field gradients.

The remainder of this paper is organized as follows: Section 2 provides the theoretical background pertaining to the modeling and characterization of an MTB, along with the characterization results of the magnetic dipole moment and the response to a field with alternating direction. Magnetic redundancy is presented in Section 3, along with the design of a null-space control system. Motion control experimental results of the PD and the null-space control systems are included in Section 4. Finally, Section 5 concludes and provides directions for future work.

2. Modeling and characterization of an MTB

The motion of an MTB in a fluid with a low Reynolds number is governed by the propulsion force of the flagella bundle, the magnetic force and torque, and the drag force and torque. The propulsion force depends on the morphology of the MTB, the dimensions of the flagella and their angular velocity, whereas the magnetic force (and torque) depends on the magnetic dipole moment of the MTB and the gradients of the induced magnetic fields. The drag force (and torque) experienced by an MTB depends on its morphology and velocity, and the dynamic viscosity of the fluid. In this section, we discuss the modeling of the MTB. In addition, characterization of the magnetic dipole moment of the MTB and its response to a field with alternating direction are also addressed.

2.1. Modeling of an MTB

The magnetic force ($\mathbf{F}(\mathbf{P}) \in \mathbb{R}^{3\times1}$) and torque ($\mathbf{T}(\mathbf{P}) \in \mathbb{R}^{3\times1}$) experienced by an MTB at position ($\mathbf{P} \in \mathbb{R}^{3\times1}$) are given by

$$\mathbf{F}(\mathbf{P}) = (\mathbf{m}\cdot\nabla)\,\mathbf{B}(\mathbf{P}) \quad \text{and} \quad \mathbf{T}(\mathbf{P}) = \mathbf{m}\times\mathbf{B}(\mathbf{P}), \tag{1}$$

where $\mathbf{m} \in \mathbb{R}^{3\times1}$ and $\mathbf{B}(\mathbf{P}) \in \mathbb{R}^{3\times1}$ are the magnetic dipole moment of the MTB and the induced magnetic field, respectively. We assume that the magnitude of the magnetic dipole moment does not depend on the spatial variation of the MTB, and $\mathbf{m}\times(\nabla\times\mathbf{B}(\mathbf{P})) = 0$ (Boyer, 1988). An MTB aligns itself along the field lines by the magnetic torque exerted on its magnetite nanocrystals, whereas the magnetic force along with the propulsion force provided by the flagella bundles allows for its navigation. Further, the drag force (F_d) and torque (T_d) are given by

$$F_\mathrm{d} = \gamma v \quad \text{and} \quad T_\mathrm{d} = \alpha\omega, \tag{2}$$

where v and ω are the linear and angular velocities of the MTB, respectively. In (2), γ is the linear drag coefficient and is given by (Berg, 1993)

$$\gamma = 2\pi\eta L\left[\ln\left(\frac{2L}{d}\right) - 0.5\right]^{-1}, \tag{3}$$

where η, L and d are the dynamic viscosity of the fluid, length and diameter of the MTB, respectively. Further, in (2), α is the rotational drag coefficient and is given by (Chemla et al., 1999)

$$\alpha = \frac{\pi\eta L^3}{3}\left[\ln\left(\frac{L}{d}\right) + 0.92\left(\frac{d}{L}\right) - 0.662\right]^{-1}. \tag{4}$$

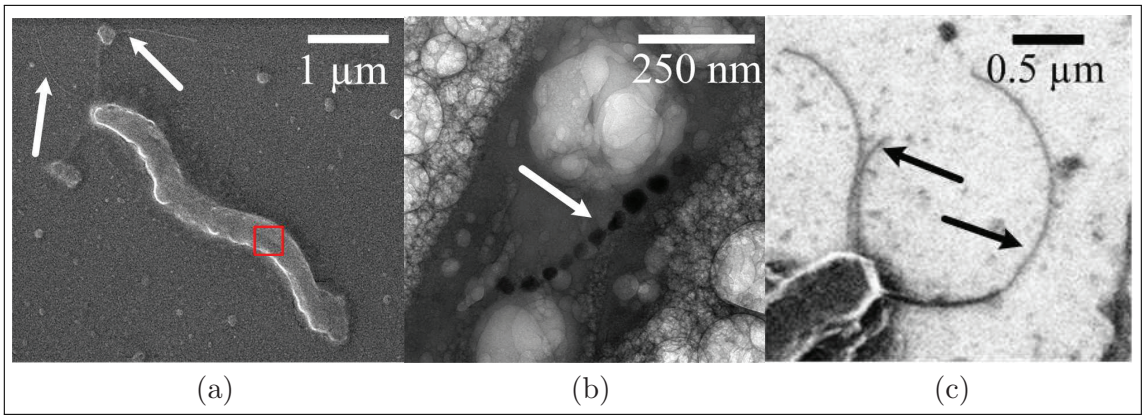

Fig. 3. Scanning/transmission electron microscopy (SEM/TEM) images of the magnetotactic bacterium (MTB), i.e. *M. magnetotacticum* (MS-1). (a) SEM image of the MTB: the MTB has a flagella bundle at its upper end. The white arrows indicate the flagella. The red square indicates the position of the magnetite nanocrystals. (b) TEM image of the magnetite nanocrystals: the membrane of the MTB envelopes chains of magnetite nanocrystals. The white arrow indicates a chain of magnetite nanocrystals. (c) SEM image of the flagella: the black arrows indicate the flagella of an MTB.

Ignoring the effect of the inertial terms, motion of the MTB is governed by

$$|\mathbf{F}(\mathbf{P})| + F_{\mathrm{d}} + f = 0 \quad \text{and} \quad |\mathbf{T}(\mathbf{P})| + T_{\mathrm{d}} + \Omega = 0, \quad (5)$$

where f and Ω are the propulsion force and torque generated by the helical flagella, respectively.

2.2. Characterization of magnetotactic bacteria

Characterization of an MTB includes the determination of its morphology, magnetic dipole moment and response to a field with alternating direction. Morphology is analyzed by the scanning electron microscopy (SEM)/TEM images of our MTB, whereas the magnetic dipole moment and the response to a field with alternating direction are characterized using a magnetic-based manipulation system (Keuning et al., 2011; Khalil et al., 2012a).

2.2.1. Magnetic-based manipulation system Our magnetic system consists of an array of orthogonally oriented metal-core electromagnets, as shown in Figure 2. This array is similar in configuration to the lower set of the OctoMag (Kummer et al., 2010), since we only consider the motion control in a planar workspace. Using this configuration, the magnetic fields are uniform within the field of view of our magnetic-based manipulation system, i.e. 300 μm $\times$ 200 μm. Uniformity of the magnetic fields within the workspace of the MTB allows us to evaluate our closed-loop control approach. Our goal is to decrease the velocity of a controlled MTB without pulling by the field gradients. Unlike the Helmholtz and Maxwell coils, each of our electromagnets has its own current amplifier (Elmo 'Whistle' 1/60 servo controllers, Elmo Motion Control, Petach-Tikva, Israel). The four independent electromagnets allow us to project an additional control input onto the null space of the magnetic force–current map of our magnetic-based manipulation system. This will be discussed in Section 3.1.

The array of electromagnets surrounds a capillary tube which incubates a culture of MTBs in 0.02 ml of growth medium. The *M. magnetotacticum* MS-1 culture is incubated in a vial with 10 ml of growth medium. After 4–10 days of incubation, MS-1 colonies are observed. The bacterial density ranges from 10^6 to 10^7/ml. The MS-1 cultures utilized in our work are grown according to the protocol provided by Bertani et al. (2001).

2.2.2. Morphology of a MTB We observe from the TEM and SEM images of our MTB that its membrane has an average diameter (d) and length (L) of 0.5 μm and 5 μm, respectively, as shown in Figure 3(a). This membrane envelopes a chain of magnetite nanocrystals with a cuboctahedral morphology with an average edge length of $\sim$36 nm (Figure 3(b)). The flagellum (Figure 3(b)) has length and thickness of 3.0 μm and 20 nm, respectively. The morphology of the MTB is determined from 15 TEM and SEM images. This data is used to calculate the rotational drag coefficient (α) using (4), and further utilized in the characterization of the magnetic dipole moment.

2.2.3. Magnetic dipole moment Under magnetic field reversals, an MTB undergoes *U-turn* trajectories. Figure 4 provides the motion of an MTB under the influence of magnetic field reversal. The MTB aligns itself and swims along the field lines ($t = 1.3$ s), and once a magnetic field reversal is initiated ($t = 2.7$ s), it undergoes a *U-turn* to align itself along the field lines, and then it swims along the field lines again ($t = 3.6$ s and $t = 5.5$ s). The diameter (D) of the *U-turn* trajectory is given by

$$D = \frac{\alpha \pi v}{|\mathbf{m}||\mathbf{B}(\mathbf{P})|}. \quad (6)$$

The diameter of the *U-turn* trajectory can be determined, then (6) can be used to calculate the magnetic dipole

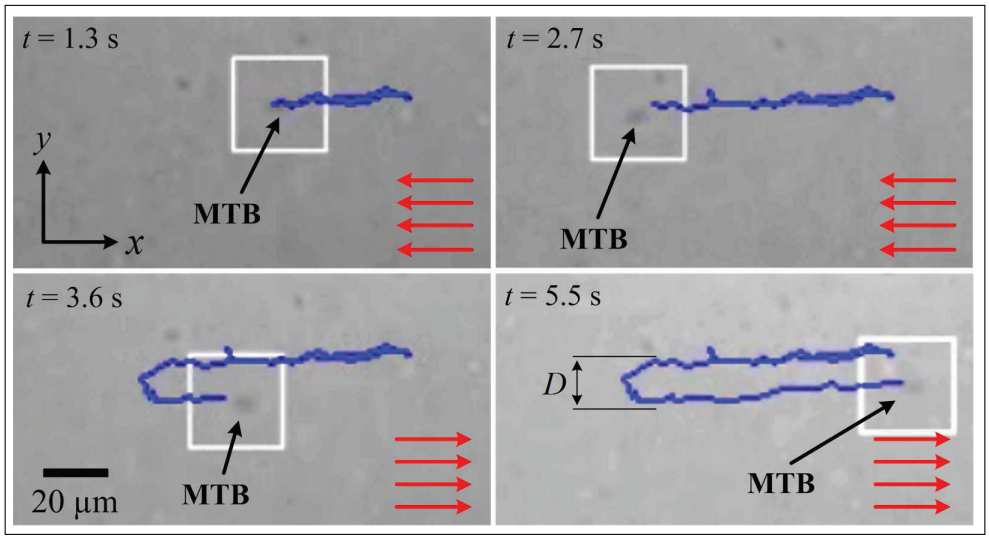

Fig. 4. The magnetotactic bacterium (MTB) undergoes a *U-turn* trajectory due to the reversal of the magnetic field. Uniform magnetic fields are applied and reversed using an electromagnet (C). The field reversal is initiated at time ($t = 2.7$ s). The red lines represent the magnetic fields before and after the magnetic field reversal. The diameter (D) of the *U-turn* is used to calculate the magnetic dipole moment using (6). The blue line indicates the path taken by the MTB. The white square is assigned by our feature tracking software to indicate the position of the MTB (Keuning et al., 2011).

moment at a specific magnetic field and based on the linear velocity of the MTB, and the properties of the growth medium. We assume that the growth medium has similar properties as water.

We utilize our magnetic-based manipulation system to generate uniform fields. Multiple reversals of these fields are performed and the corresponding diameters of the *U-turn* trajectories are determined, as shown in Figure 5. The average *U-turn* diameter is $\sim$15 μm from 15 MTBs. Using (6), the magnetic dipole moment of the MTB has an average of 3.11×10^{-16} A m^2 at magnetic field of 7.9 mT. This characterization agrees with the results reported by Bahaj et al. (1996).

2.2.4. Frequency response of MTBs The characterized magnetic dipole moment of the MTB has an order-of-magnitude of 10^{-16}. In order to provide a pulling force to overcome the propulsion force generated by the flagella, we have to use relatively large field gradients (Martel et al., 2009). This pulling force is required to increase the positioning accuracy of the control system by decreasing the velocity of the MTB within the vicinity of a reference position. The magnitude of the maximum magnetic field gradients that can be generated by our magnetic-based manipulation system is 60 mT/m. Therefore, the pulling magnetic force is at least five orders-of-magnitude less than the force generated by the flagella of the MTB. Instead of using field gradients, we apply a field with alternating direction (Figure 6) with a frequency range of 0 Hz to 100 Hz. The magnetic torque generated by the field with alternating direction enforces the MTB to align itself along the alternating field lines. Such response could perturb the modes of its flagella, and hence decrease its linear velocity. In order to verify that a field with alternating direction indeed decreases the linear velocity of the MTB, we apply this field and measure the corresponding average velocity of the MTB at each frequency.

Electromagnets A and C are used to generate uniform fields, while sinusoidal current inputs are simultaneously applied to electromagnets B and D to alternate the direction of the uniform fields generated by electromagnets A and C. Figure 6 shows a finite element (FE) simulation of the magnetic field with alternating direction. This field allows the MTB to swim parallel to the x-axis of our magnetic-based manipulation system. We detect the position of the MTB using a feature tracking software (Keuning et al., 2011). Figure 7 provides the motion of the MTB along the x-axis (motion along the y-axis is almost zero) for a field-with-alternating direction with a frequency range of 0 to 100Hz. We calculate the velocity by differentiating the position of the MTB, followed by applying a low-pass filter. We observe that the linear velocity of the MTB decreases as we increase the frequency of the field with alternating direction. We repeat this experiment for 10 different MTBs to determine the frequency response. The frequency response of our MTB is provided in Figure 8. This characterization result indicates that the linear velocity of the MTB decreases as we increase the frequency of the field with alternating direction. We observe that the average velocity of the MTB decreases by 37% at a frequency of 85 Hz. In this characterization experiment, the angle of the field

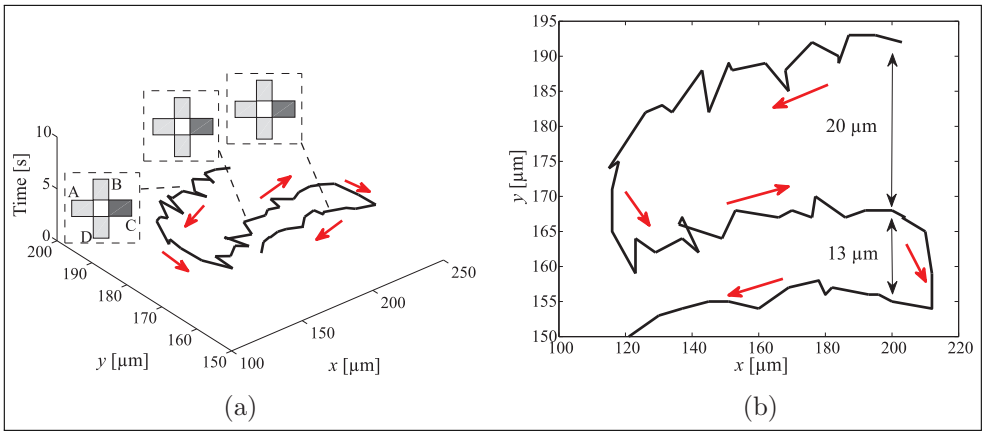

Fig. 5. Characterization of the magnetic dipole moment using the *U-turn* technique. The average diameter (∼15 μm) of the *U-turn* trajectories is used to calculate the magnetic dipole moment of the magnetotactic bacterium (MTB). The average is calculated from 15 MTBs. The magnetic dipole moment has an average of 3.11×10^{-16} A m^2 at a magnetic field of 7.9 mT. Magnetic dipole moment is calculated using (6). (a) Motion of the MTB during reversals of the magnetic fields using electromagnet C. The electromagnets are labeled with the letters A, B, C and D. Electromagnet C (darker shade) is active during this characterization experiment. (b) The average diameter of the *U-turn* trajectories is calculated from the motion analysis of the MTB. The red arrows indicate the motion of the MTB.

with alternating direction is 90° to maximize the exerted magnetic torque on the magnetite nanocrystals of the MTB.

The frequency response of the MTB allows us to control its linear velocity without field gradients. This control can be achieved by applying a field with alternating direction which points towards a given reference position. Frequency of this field depends on the frequency response of the MTB, i.e. a specific frequency can be devised based on the desired linear velocity of the MTB. Our null-space control system benefits from such response to increase the positioning accuracy of the MTB.

3. Control system design

Point-to-point positioning of an MTB can be achieved by directing the fields towards a reference position. However, due to the self-propulsion provided by the flagella of the MTB, this control only positions the MTB within the vicinity of the reference position, i.e. region of convergence. The positioning accuracy of the MTB can be increased by decreasing its velocity to decrease the size of the region of convergence. Our control system is based on the superposition of two inputs, the first input generates uniform fields which points towards a given reference position. The second input causes these fields to alternate. This superposition results in a field with alternating direction which points towards a given reference position. This control can be realized by projecting one of the control inputs onto the null-space of the force–current map of our redundant magnetic-based manipulation system.

3.1. Redundancy of magnetic-based manipulation systems

Consider a magnetic-based manipulation system with n-electromagnets, the magnetic field at a point can be determined by the superposition of the contribution of the ith electromagnet (Kummer et al., 2010)

$$\mathbf{B}(\mathbf{P}) = \sum_{i=1}^{n} \mathbf{B}_i(\mathbf{P}), \tag{7}$$

where $\mathbf{B}(\mathbf{P}) \in \mathbb{R}^{3\times 1}$ and $\mathbf{B}_i(\mathbf{P})$ are the induced magnetic field at a point ($\mathbf{P} \in \mathbb{R}^{3\times 1}$) and the induced magnetic field by the ith electromagnet, respectively. Linearity of the magnetic field and the current allows us to rewrite (7) as follows (Khalil et al., 2012b):

$$\mathbf{B}(\mathbf{P}) = \sum_{i=1}^{n} \widetilde{\mathbf{B}}_i(\mathbf{P})\, I_i = \widetilde{\mathbf{B}}(\mathbf{P})\, \mathbf{I}, \tag{8}$$

where $\widetilde{\mathbf{B}}(\mathbf{P}) \in \mathbb{R}^{3\times n}$ is a matrix which depends on the position at which the magnetic field is evaluated, and $\mathbf{I} \in \mathbb{R}^{n\times 1}$ is a vector of the applied current. The magnetic field due to each electromagnet is related to the current input (I_i) by $\widetilde{\mathbf{B}}_i(\mathbf{P})$. Substituting (8) in (1) yields the following magnetic force–current map:

$$\mathbf{F}(\mathbf{P}) = (\mathbf{m} \cdot \nabla)\, \widetilde{\mathbf{B}}(\mathbf{P})\mathbf{I} = \mathbf{\Lambda}(\mathbf{m}, \mathbf{P})\, \mathbf{I}, \tag{9}$$

where $\mathbf{\Lambda}(\mathbf{m}, \mathbf{P}) \in \mathbb{R}^{3\times n}$ is the actuation matrix which maps the input current to the magnetic force. The matrix $\mathbf{\Lambda}(\mathbf{m}, \mathbf{P})$ has three linearly independent rows. Therefore, it can control three independent degrees of freedom. There exists several magnetic-based manipulation systems in which the number of linearly independent resultant magnetic forces is greater than the number of linearly independent degrees of freedom of the magnetically guided object (Kratochvil et al., 2010; Kummer et al., 2010; Khalil et al., 2012a). Such systems can be considered as redundant magnetic-based manipulation systems.

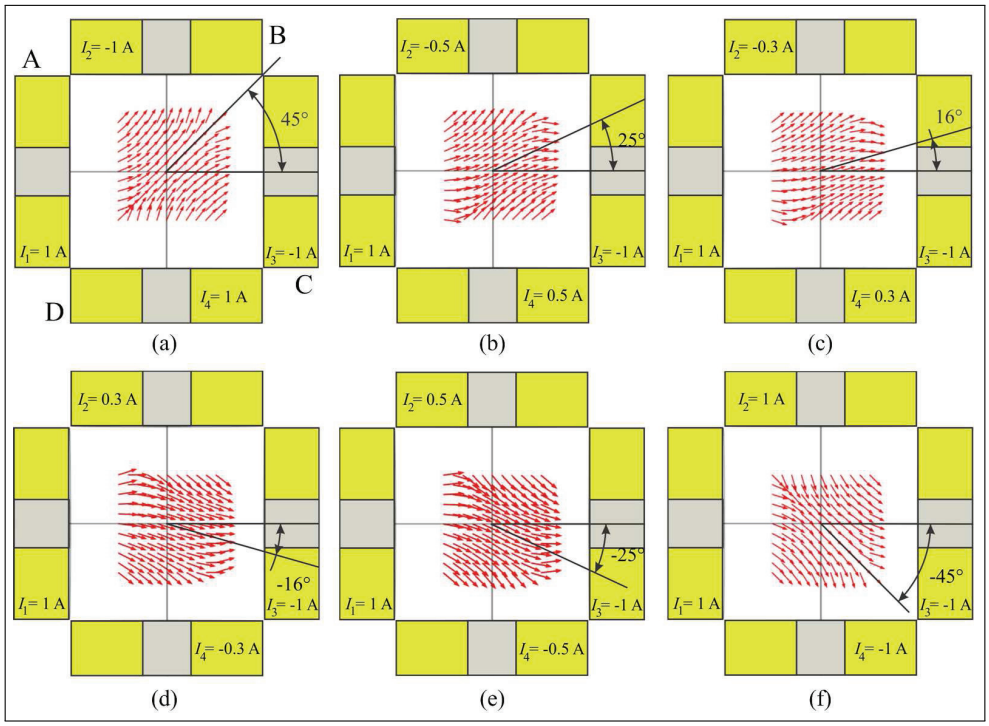

Fig. 6. Finite element (FE) simulation of six representative cases for the field with alternating direction utilized in the frequency response characterization. Electromagnets A and C are used to generate uniform magnetic fields (within the center of the workspace), whereas electromagnets B and D are used to alternate the direction of these fields. Electromagnets A and C are supplied with constant currents (I_1 and I_3) of 1 A and −1 A, respectively. Electromagnets B and D are supplied simultaneously with sinusoidal current inputs. I_i for ($i = 1, \ldots, 4$), denotes the current at each of the electromagnets: (a) $I_2 = -1$ A and $I_4 = 1$ A; (b) $I_2 = -0.5$ A and $I_4 = 0.5$ A; (c) $I_2 = -0.3$ A and $I_4 = 0.3$ A; (d) $I_2 = 0.3$ A and $I_4 = -0.3$ A; (e) $I_2 = 0.5$ A and $I_4 = -0.5$ A; (f) $I_2 = 1$ A and $I_4 = -1$ A. The angle of the field with alternating direction is 90° within the center of the workspace of our magnetic-based manipulation system. The frequency of this field is varied from 0 to 100 Hz. The FE model is created using ComsolMultiphysics® (COMSOL, Inc., Burlington, USA).

Definition 1 *In magnetic-based manipulation systems, when the number of linearly independent resultant magnetic forces is greater than the number of linearly independent degrees of freedom of a magnetically guided object, the magnetic system is said to be magnetically redundant.*

Redundancy of a magnetic-based manipulation system refers to the presence of more electromagnets than the number of linear independent degrees of freedom of a magnetically guided object, e.g. magnetic micro- and nanoparticles, microrobot (Zhang et al., 2009; Valdastri et al., 2011) and magnetic microorganisms.

Definition 2 *The difference between the number of electromagnets within a redundant magnetic system and the number of linearly independent degrees of freedom of a magnetically guided object, is the degree of magnetic redundancy.*

Redundancy of a magnetic-based manipulation system allows for the projection of an auxiliary control input onto the null-space of the actuation matrix of its magnetic force–current map (9). This null-space control input does not affect the main task of the control system (Khatib, 1987). Therefore, our closed-loop control approach employs redundancy of the magnetic-based manipulation system to provide two control inputs. The first is applied such that the generated fields are oriented towards a reference position, whereas the second is a null-space control input. The null-space control input alternates the direction of the fields generated by the first input. The superposition of these two input results in a field with alternating direction, which points towards a given reference position. This field allows us to change the velocity of the MTB based on the frequency response analysis (Section 2.2.4).

Our magnetic-based manipulation system (Figure 2) is developed to control the motion of an MTB in a planar workspace. This system allows for the control of three degrees of freedom of the MTB (two planar and one rotational). Therefore, our magnetic-based manipulation system has a single degree of magnetic redundancy (Definition 2).

Realization of the aforementioned control system requires the evaluation of the actuation matrix ($\mathbf{\Lambda}(\mathbf{m}, \mathbf{P})$)

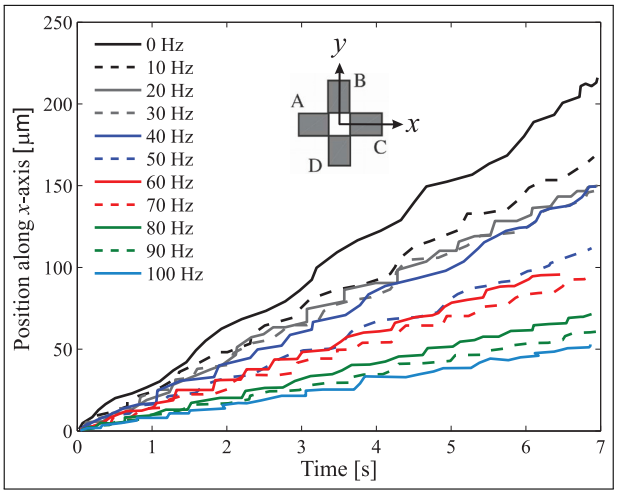

Fig. 7. Position of the magnetotactic bacterium (MTB) versus time in the presence and absence of a field with alternating direction. The frequency of this field ranges from 0 to 100 Hz. Electromagnets A and C are used to generate uniform magnetic fields, whereas electromagnets B and D are used to alternate the direction of the fields generated by electromagnets A and C, to generate a field with alternating direction. Position of the MTB along the y-axis is almost zero. This experiment is repeated using 10 different MTBs to characterize the frequency response of the MTB. Position of the MTB is detected using a feature tracking software (Keuning et al., 2011).

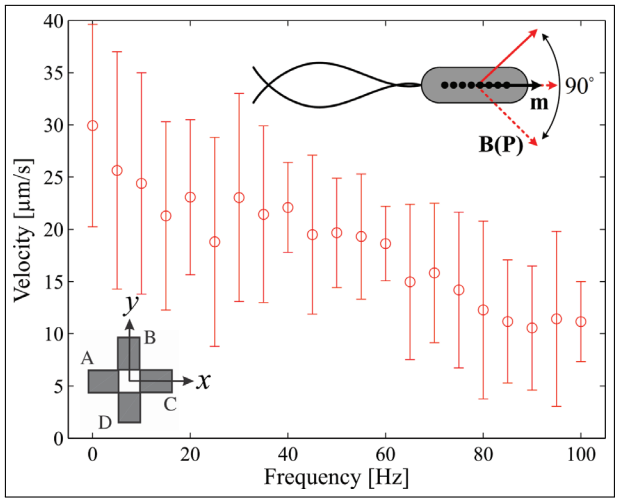

Fig. 8. Response of the magnetotactic bacterium (MTB) to a field with alternating direction. The frequency response analysis indicates that the linear velocity of the MTB decreases by 37% at a field frequency of 85 Hz. This characterization experiment is done by applying a field with alternating direction (shown by the solid and dashed red arrows in the inset at the upper right corner), and calculating the average velocity of the MTB at each frequency. The magnetic dipole moment ($\mathbf{m}$) allows the MTB to align itself along the field with alternating direction. This field is generated by producing uniform magnetic fields using electromagnets A and C. The direction of these fields is altered by applying sinusoidal current input simultaneously to electromagnets B and D. The electromagnets are provided by the inset at the bottom left corner. The angle of the field with alternating direction is 90°. The average velocity is calculated from 10 different MTBs at each frequency. The maximum magnetic field strength is 2 mT.

and its pseudo-inverse. This matrix depends on the magnetic dipole moment of the MTB, and its position. We have shown that the dipole moment can be characterized from the motion analysis of the MTB during the reversal of the magnetic field (Section 2.2.3). We use the FE model of our magnetic-based manipulation system, and calculate the gradients of the magnetic fields within a 1 mm × 1 mm workspace (Figure 9). This region spans the workspace of the MTB. We apply 16 sets of current vectors and calculate the corresponding gradients at each time. These current sets are devised based on the saturation limits of our current amplifiers. The calculated gradients are provided in Figure 9, for one set of current inputs of $[0.1 \;\; 0.2 \;\; 0.3 \;\; 0.4]^{\mathrm{T}}$ A. We observe from the FE analysis that the gradients of the magnetic fields are almost constant within a limited region of the workspace of our magnetic-based manipulation system. Such observation simplifies the control system since the actuation matrix and its pseudo-inverse do not have to be evaluated at every point in the workspace. Although we devise a null-space control input as a sinusoidal input, the field gradients within the center of the workspace are almost constant. Within this limited workspace, the null-space input only causes the direction of the fields, generated by the first control input, to alternate. Alternating the direction of the fields allows us to control the position of the MTB and decrease its linear velocity based on its characterized frequency response.

3.2. *Null-space control*

In order to realize the null-space control system of the MTB, we calculate the position and velocity tracking errors as follows:

$$\mathbf{e} = \mathbf{P} - \mathbf{P_{ref}} \quad \text{and} \quad \dot{\mathbf{e}} = \dot{\mathbf{P}} - \dot{\mathbf{P}}_{\mathbf{ref}} = \dot{\mathbf{P}}, \tag{10}$$

where $\mathbf{e}$ and $\dot{\mathbf{e}}$ are the position and velocity tracking errors, respectively. Further, $\mathbf{P_{ref}}$ is a fixed reference position. We devise a desired magnetic force ($\mathbf{F_{des}(P)}$) of the form

$$\mathbf{F_{des}(P)} = \mathbf{K_p e} + \mathbf{K_d}\dot{\mathbf{e}}. \tag{11}$$

In (11), $\mathbf{K_p}$ and $\mathbf{K_d}$ are the controller positive-definite gain matrices, and are given by

$$\mathbf{K_p} = \begin{bmatrix} k_{\mathrm{p1}} & 0 \\ 0 & k_{\mathrm{p2}} \end{bmatrix} \text{ and } \mathbf{K_d} = \begin{bmatrix} k_{\mathrm{d1}} & 0 \\ 0 & k_{\mathrm{d2}} \end{bmatrix}, \tag{12}$$

where $k_{\mathrm{p}i}$ and $k_{\mathrm{d}i}$, for ($i = 1, 2$), are the proportional and derivative gains, respectively. Substituting (11) in the force equation (5), and assuming no propulsion force ($f = 0$) yields the following position tracking error dynamics:

$$\dot{\mathbf{e}} + (\mathbf{K_d} + \gamma \mathbf{\Pi})^{-1} \mathbf{K_p e} = 0, \tag{13}$$

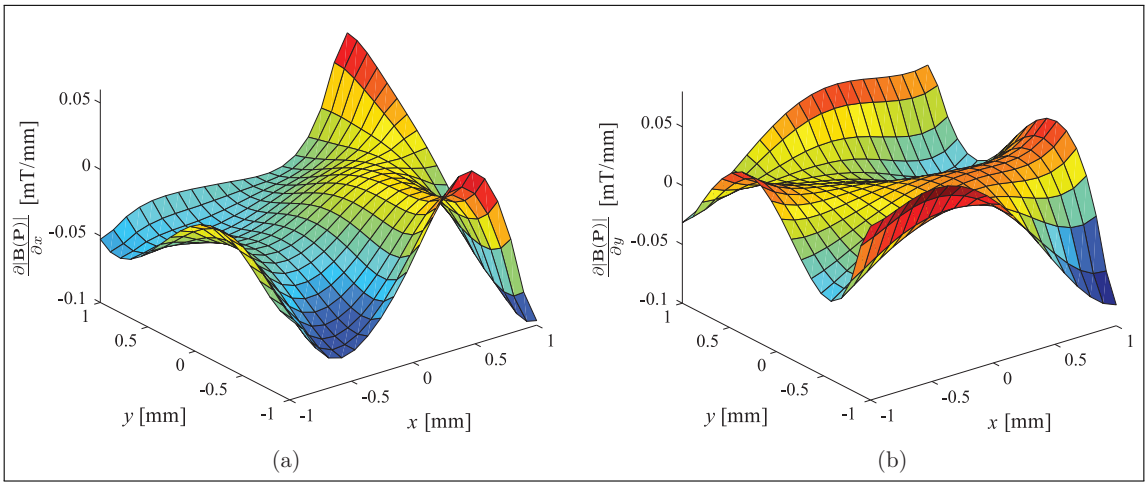

Fig. 9. Magnetic field gradients throughout an area of 1 mm × 1 mm within the center of the workspace of our magnetic-based manipulation system (Figure 2). (a) Field gradient with respect to x-axis. (b) Field gradient with respect to y-axis. The gradients are calculated from the magnetic fields generated by a finite element (FE) model of our system.The field gradients are calculated when a current vector of $[0.1 \quad 0.2 \quad 0.3 \quad 0.4]^{\mathrm{T}}$ A is applied. The entries of this current vectors are applied to electromagnets A, B, C and D, respectively. The FE analysis demonstrates that the field gradients are almost constant within the center of the workspace (this region is approximately twice larger than our field of view). Therefore, the actuation matrix is assumed constant within this region. The FE model is created using Comsol Multiphysics® (COMSOL, Inc., Burlington, USA).

where $\mathbf{\Pi}$ is the identity matrix with the proper dimension. Since $f \neq 0$, zero position tracking error cannot be achieved. However, the control system locates the MTB within the vicinity of the reference position based on (13). Therefore, the accuracy of the control system can be evaluated through the size of the region of convergence in which the MTB is positioned by the closed-loop control system. Owing to the magnetic redundancy of our magnetic-based manipulation system, an auxiliary control input ($\mathbf{\Gamma}$) can be projected onto the null-space of the actuation matrix without affecting the main task of the motion control. Thus, the solution of (9) is

$$\mathbf{I} = \mathbf{\Lambda}(\mathbf{m},\mathbf{P})^{\dagger}\,\mathbf{F_{des}}(\mathbf{P}) + \left(\mathbf{\Pi} - \mathbf{\Lambda}(\mathbf{m},\mathbf{P})^{\dagger}\,\mathbf{\Lambda}(\mathbf{m},\mathbf{P})\right)\mathbf{\Gamma}. \tag{14}$$

The first term of (14) orients the MTB towards the reference position based on (13), while the auxiliary control input $\mathbf{\Gamma}$ is projected onto the null-space of $\mathbf{\Lambda}(\mathbf{m},\mathbf{P})$ by the null-space projection matrix $\left(\mathbf{\Pi} - \mathbf{\Lambda}(\mathbf{m},\mathbf{P})^{\dagger}\,\mathbf{\Lambda}(\mathbf{m},\mathbf{P})\right)$.

Based on the frequency response characterization (Section 2.2.4), we devise a sinusoidal null-space control input. Frequency of this sinusoidal input depends on the frequency response of the MTB, and its desired linear velocity. It is important to note that the first term of (14) is a PD control input. This input controls the direction of the field lines to orient the MTB towards the reference position. The second term of (14) alternates the direction of the fields generated by the first input. The resulting field with alternating direction perturbs the modes of the flagella and hence, decreases its velocity.

4. Experimental results

The motion control experimental results are carried out on the magnetic-based manipulation system, shown in Figure 2. This system has four electromagnets and a single degree of magnetic redundancy. This redundancy allows for the projection of the auxiliary control input ($\mathbf{\Gamma}$) onto the null-space of $\mathbf{\Lambda}(\mathbf{m},\mathbf{P})$. In order to verify that the null-space control law (14) indeed achieves relatively higher positioning accuracy than a PD control system, we perform *point-to-point* positioning for two cases. The first is performed using only the first term of (14), i.e. PD control system, while the second is the overall control law (14). The average linear velocity and region of convergence are used to evaluate the performance of the control systems. The average is calculated from 10 different trials for the same controller gains. The comparison between these two control systems is done using MTBs from the same culture, since the magnetic properties of the MTBs affects the accuracy of the control system.

4.1. Case I: PD control

In this experiment, two reference positions are tracked using the first term of the control law (14). This control law orients the MTB towards the reference positions (shown by the blue circles), then the MTB performs flagellated motion towards these reference positions, as shown in Figure 10(a). The PD control system does not have any influence on the linear velocity of the MTB. We observe that the MTB follows the given reference positions at an average velocity of 29 μm s^{-1}. In addition, the PD control system positions the

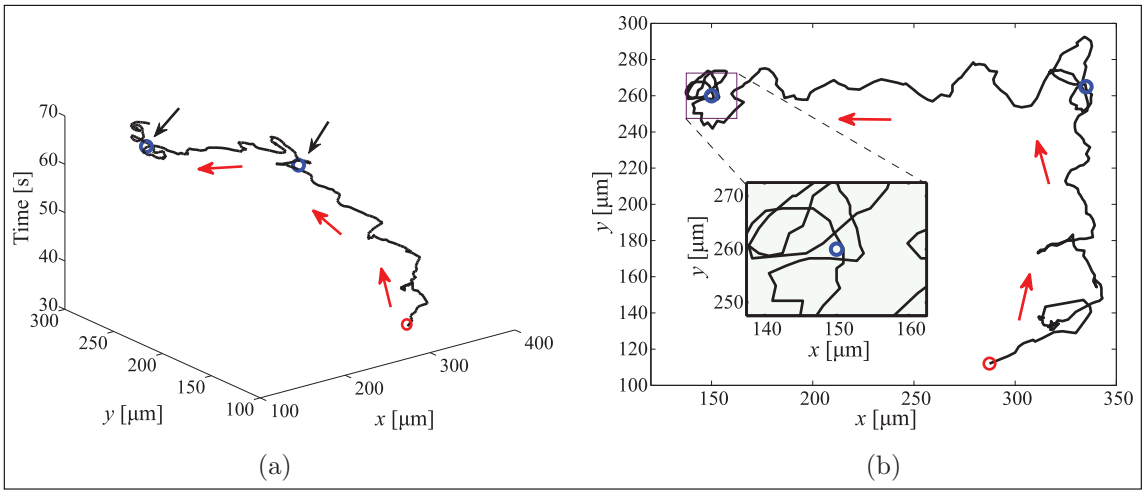

Fig. 10. Case I: *point-to-point* closed-loop control of a magnetotactic bacterium (MTB) under the influence of the magnetic fields. The MTB is controlled using the first term of (14), i.e. a proportional-derivative (PD) control law. The controller gains are $k_{p1} = k_{p2} = 15.0\ \mathrm{s}^{-2}$ and $k_{d1} = k_{d2} = 15.5\ \mathrm{s}^{-1}$. The PD control system positions the MTB at an average velocity of 29 μm s^{-1} within an average region of convergence of 26 μm in diameter. (a) The MTB follows two reference positions using a PD control law. (b) The inset indicates the effect of the PD control system on the motion of the MTB within the vicinity of the second reference position. The blue circles indicate the reference positions. The black arrows indicate the reference positions, whereas the red arrows indicate the direction of the MTB.

MTB within a region of convergence of 26 μm in diameter. The inset in Figure 10(b) provides the response of the controlled MTB within the vicinity of the second reference position.

4.2. Case II: null-space control

The null-space control law (14) consists of two inputs. The first input is a PD control law, whereas the second is an auxiliary input. Our objective is to decrease the velocity of the MTB to increase its positioning accuracy. We devise a field with alternating direction at frequencies from 1 to 5 Hz. As shown in Figure 11(a), the MTB follows two reference positions (shown by the blue circles) under the influence of the controlled magnetic fields. These fields orient the MTB towards the reference position while simultaneously decreasing its linear velocity by the field with alternating direction at frequency of 5 Hz. The average velocity and average diameter of the region of convergence are 15 μm s^{-1} and 13 μm, respectively. Figure 11(b) provides the response of the controlled MTB within the vicinity of the first reference position (shown by the inset).

Table 1 provides a comparison between the PD and the null-space control systems of the MTB (the null-space control system is implemented at five frequencies for the null-space input). Projecting the control input Γ onto the null-space of the actuation matrix $(\mathbf{\Lambda}(\mathbf{m}, \mathbf{P}))$ decreases the linear velocity and the region of convergence of the MTB. The percentage of decrease depends on the frequency of the null-space control input. Therefore, the design of the null-space control system depends on three sets of controller gains, i.e. the proportional gains, the derivative gains and the frequency of the null-space input. The first two sets of controller gains must be selected such that stable position tracking error is achieved based on (13), whereas the frequency of the null-space input can be chosen based on the desired linear velocity of the MTB, and based on its characterized frequency response.

The average velocity of the controlled MTB for the null-space control input of 5 Hz is less than the average velocity provided by the frequency response of the MTB for the same frequency (Figure 8). This is due to the open-loop nature of the frequency response characterization experiment, whereas Table 1 provides the characteristics of closed-loop controlled MTB.

5. Discussion

Frequency of a field with alternating direction has a greater influence on the velocity of the MTB than the gains of the control system. Increasing these gains to generate larger field gradients is not feasible, not only due to the practical limitations on the generation of magnetic field gradients (Abbott et al., 2009; Nelson et al., 2010), but also due to the value of the magnetic dipole moment of the MTB (order of magnitude of 10^{-16}). Our study presents a closed-loop control approach. This approach allows us to control the direction and the velocity of the MTB. The direction is controlled by orienting the fields towards the reference position, while the velocity is decreased by alternating the direction of the fields based on the frequency response of the MTB. This approach benefits from the magnetic redundancy of magnetic-based manipulation systems. This redundancy allows for the projection of an auxiliary

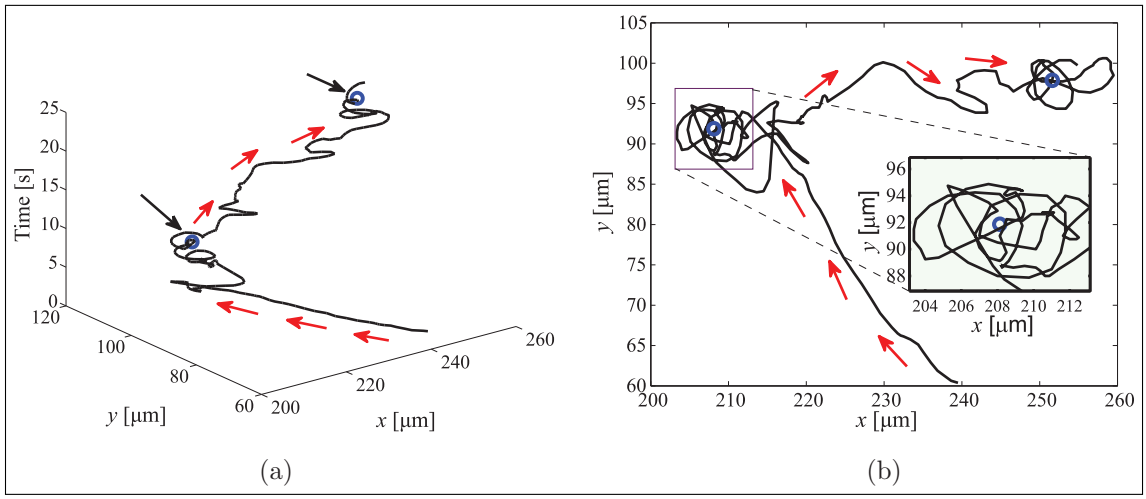

Fig. 11. Case II: *point-to-point* closed-loop control of a MTB under the influence of the magnetic fields. The MTB is controlled using the null-space control law (14). The controller gains are $k_{p1} = k_{p2} = 15.0\ s^{-2}$ and $k_{d1} = k_{d2} = 15.5\ s^{-1}$ and the field with alternating direction is applied at a frequency of 5 Hz. The null-space control system positions the MTB at an average velocity of 15 μm s^{-1} within a region of convergence of 13 μm. (a) MTB follows two reference positions using the null-space control system. (b) The inset indicates the effect of the null-space control system on the motion of the MTB within the vicinity of the first reference position. The blue circles indicate the reference positions. The black arrows indicate the reference positions, whereas the red arrows indicate the direction of the MTB.

input onto the null-space of the projection matrix of the magnetic force–current map. Although we devise an auxiliary input which generates field with alternating direction, redundancy of magnetic-based manipulation systems allows for the projection of different inputs.

The null-space control system is evaluated at frequencies from 1 to 5 Hz to demonstrate the effect of the field with alternating direction on the controlled MTB. Although this field results in a decrease in the velocity of the MTB and a corresponding increase in the positioning accuracy, greater frequencies can be applied based on the frequency response analysis (Section 2.2.4), to provide different transient- and steady-state characteristics of the controlled MTB.

The positioning accuracy depends on the magnetic dipole moment of the MTB. Our closed-loop control system positions an MTB within the vicinity of the reference position by reversing the direction of the magnetic fields to decrease the position tracking error. Therefore, within the vicinity of the reference position an MTB undergoes *U-turn* trajectories (as shown in the insets of Figure 10 and Figure 11). The time of a *U-turn* is given by (Esquivel and Lins de Barros, 1986)

$$\tau = \frac{\alpha}{|\mathbf{m}||\mathbf{B}(\mathbf{P})|} \ln\left(\frac{2|\mathbf{m}||\mathbf{B}(\mathbf{P})|}{\mathrm{k}T}\right), \qquad (15)$$

where τ is the time of the *U-turn* trajectory. Further, k and T are the Boltzmann constant and the temperature of the fluid, respectively. Based on (15), the bacterial culture with larger magnetic dipole moment undergoes *U-turn* trajectories in a shorter time.

During the preparation of the magnetotactic bacteria cultures (of the same strain), we observe that their magnetic dipole moment varies even when we follow the same culturing protocol (Bertani et al., 2001). In a prior study (Khalil et al., 2012c), we showed that the characterized magnetic dipole moment of the strain *M. magnetotacticum* MS-1 is 3.32×10^{-16} A m^{-2}. In our current work, the characterized magnetic dipole moment of the same bacterial strain is 3.11×10^{-16} A m^{-2}. Based on (15), the magnetic dipole moment affects the time of the *U-turn* trajectories taken by a controlled MTB within the vicinity of a reference position. Therefore, the positioning accuracy can be improved by culturing bacterial strain with larger magnetic dipole moment.

5.1. Conclusions

We present a null-space control system based on the characterization of the MTB, and the redundancy of magnetic-based manipulation systems. The magnetic dipole moment is characterized using the *U-turn* technique based on the motion analysis of the MTB. The characterized magnetic dipole moment is used in the realization of the force–current map of our magnetic-based manipulation system. Characterization of the frequency response of the MTB shows that its linear velocity decreases by 37% at a field with alternating direction of frequency of 85 Hz. These characterization results are used to devise a null-space control system which controls the direction of the MTB while changing its linear velocity based on its characterized frequency response. The null-space control system allows the MTB to converge to a smaller region of convergence within the vicinity of the reference position, as opposed to a PD control system for the same controller

Table 1. Characteristics of the proportional-derivative (PD) and the null-space control systems in the transient- and steady-state. Transient-state is evaluated by the average velocity of the MTB, whereas steady-state is evaluated by the average diameter of the region of convergence (ROC). The average velocity of the MTB and the average diameter of the ROC are calculated from 10 different motion control trials for each case. Case I: PD control system. Case II: Null-space control system. The gains of the control systems are $k_{p1} = k_{p2} = 15.0\ s^{-2}$ and $k_{d1} = k_{d2} = 15.5\ s^{-1}$. The null-space control system is evaluated at five frequencies for the null-space input.

Characteristics	PD control	Null-space control				
		1 Hz	2 Hz	3 Hz	4 Hz	5 Hz
Average velocity ($\mu m\ s^{-1}$)	29 ± 10	23 ± 5	21 ± 5	20 ± 6	18 ± 5	15 ± 5
ROC (μm)	26 ± 8	22 ± 6	21 ± 7	19 ± 5	17 ± 6	13 ± 6

gains. The region of convergence achieved by the null-space control system (at frequency of 1 Hz of the null-space input) is 15% smaller than the region of convergence of the PD control system. The experimental results demonstrate that increasing the frequency of the null-space input by 1 Hz, enhances the positioning accuracy by decreasing the region of convergence and the linear velocity of the MTB by ∼10%.

5.2. Future work

Characterization and control of the MTB in three-dimensional space will be studied. Our magnetic-based manipulation system will be redesigned to allow for the visual tracking, auto-focusing and control of the MTB in three-dimensional space. *In vivo* experiments are essential to study the effect of the fluidic-flow rates and the time-varying fluid viscosity. These experiments necessitate the utilization of a clinical imaging modality, such as magnetic resonance imaging (Martel et al., 2009a). In addition, closed-loop control of a swarm of MTBs will be studied.

Funding

This work was partially supported by funds from MIRA-Institute for Biomedical Technology and Technical Medicine, University of Twente, The Netherlands.

References

Abbott JJ, Peyer KE, Lagomarsino MC, et al. (2009) How should microrobots swim? *The International Journal of Robotics Research* 28: 1434–1447.

Bahaj AS and James PAB (1993) Characterisation of magnetotactic bacteria using image processing techniques. *IEEE Transactions on Magnetics* 29: 3358–3360.

Bahaj AS, James PAB and Moeschler FD (1996) An alternative method for the estimation of the magnetic moment of non-spherical magnetotactic bacteria. *IEEE Transactions on Magnetics* 32: 5133–5135.

Berg HC (1993) *Random Walks in Biology*. Princeton, NJ: Princeton University Press.

Bertani LE, Weko J, Phillips KV, Gray RF and Kirschvink JL (2001) Physical and genetic characterization of the genome of *Magnetospirillum magnetotacticum*, strain MS-1. *International Journal on Genes and Genomes* 264: 257–263.

Blakemore RP (1975) Magnetotactic bacteria. *Science* 190: 377–379.

Boyer TH (1988) The force on a magnetic dipole. *American Journal of Physics* 56: 688–692.

Chemla YR, Grossman HL, Lee TS, Clarke J, Adamkiewicz M and Buchanan BB (1999) A new study of bacterial motion: superconducting quantum interference device microscopy of magnetotactic bacteria. *Biophysical Journal* 76: 3323–3330.

Darnton N, Turner L, Breuer K and Berg HC (2004) Moving fluid with bacterial carpets. *Biophysical Journal* 86: 1863–1870.

Erglis K, Wen Q, Ose V, et al. (2007) Dynamics of magnetotactic bacteria in a rotating magnetic field. *Biophysical Journal* 93: 1402–1412.

Esquivel DMS and Lins de Barros HGP (1986) Motion of magnetotactic microorganisms. *Journal of Experimental Biology* 121: 153–163.

Keuning JD, de Vries J, Abelmann L and Misra S (2011) Image-based magnetic control of paramagnetic microparticles in water. In *Proceedings of the IEEE/RSJ International Conference of Robotics and Systems (IROS)*, pp. 421–426.

Khalil ISM, Keuning JD, Abelmann L and Misra S (2012a) Wireless magnetic-based control of paramagnetic microparticles. In *Proceedings of the IEEE RAS/EMBS International Conference on Biomedical Robotics and Biomechatronics (BioRob)*, pp. 460–466.

Khalil ISM, Metz RMP, Abelmann L and Misra S (2012b) Interaction force estimation during manipulation of microparticles. In *Proceedings of the IEEE International Conference of Robotics and Systems (IROS)*, pp. 950–956.

Khalil ISM, Pichel MP, Zondervan L, Abelmann L and Misra S (2012c) Characterization and control of biological microrobots. In *Proceedings of the 13th International Symposium on Experimental Robotics* (*Springer Tracts in Advanced Robotics*). Berlin: Springer.

Khatib O (1987) A unified approach for motion and force control of robot manipulators: the operational space formulation. *IEEE Journal of Robotics and Automation* 3(1): 43–53.

Kratochvil BE, Kummer MP, Erni S, et al. (2010) MiniMag: a hemispherical electromagnetic system for 5-DOF wireless micromanipulation. In *Proceedings of the 12th International Symposium on Experimental Robotics* (*Springer Tracts in Advanced Robotics*). Berlin: Springer.

Kummer MP, Abbott JJ, Kratochvil BE, Borer R, Sengul A and Nelson BJ (2010) OctoMag: an electromagnetic system

for 5-DOF wireless micromanipulation. *IEEE Transactions on Robotics* 26: 1006–1017.

Lu Z and Martel S (2006) Preliminary investigation of bio-carriers using magnetotactic bacteria. In *Proceedings of the International Conference of the IEEE Engineering in Medicine and Biology Society (EMBC)*, pp. 3415–3418.

Martel S, Felfoul O, Mathieu J-B, et al. (2009) MRI-based medical nanorobotic platform for the control of magnetic nanoparticles and flagellated bacteria for target interventions in human capillaries. *The International Journal of Robotics Research* 28: 1169–1182.

Martel S, Mathieu J-B, Felfoul O, et al. (2004) Adapting MRI systems to propel and guide microdevices in the human blood circulatory system. In *Proceedings of the International Conference of the IEEE Engineering in Medicine and Biology Society (EMBC)*, pp. 1044–1047.

Martel S and Mohammadi M (2010) Using a swarm of self-propelled natural microrobots in the form of flagellated bacteria to perform complex micro-assembly tasks. In *Proceedings of the IEEE International Conference on Robotics and Automation (ICRA)*, pp. 500–505.

Martel S, Mohammadi M, Felfoul O, Lu Z and Pouponneau P (2009b) Flagellated magnetotactic bacteria as controlled MRI-trackable propulsion and steering systems for medical nanorobots operating in the human microvasculature. *The International Journal of Robotics Research* 28: 571–582.

Martel S, Tremblay CC, Ngakeng S and Langlois G (2006) Controlled manipulation and actuation of micro-objects with magnetotactic bacteria. *Applied Physics Letters* 89: 3904.

Mathieu J-B, Martel S, Yahia LH, Soulez G and Beaudoin G (2003) MRI systems as a mean of propulsion for a microdevice in blood vessels. In *Proceedings of the International Conference of the IEEE Engineering in Medicine and Biology Society (EMBC)*, vol. 4: 3419–3422.

Nelson BJ, Kaliakatsos IK and Abbott JJ (2010) Microrobots for minimally invasive medicine. *The Annual Review of Biomedical Engineering* 12: 55–85.

Nogueira FS and Lins De Barros HGO (1995) Study of the motion of magnetotactic bacteria. *European Biophysics Journal* 24: 13–21.

Sakar MS, Steager EB, Kim DH, et al. (2011) Modeling, control and experimental characterization of microbiorobots. *The International Journal of Robotics Research* 30: 647–658.

Steinberger B, Petersen N, Petermann H and Wiess DG (1994) Movement of magnetic bacteria in time-varying magnetic fields. *Journal of Fluid Mechanics* 273: 189–211.

Valdastri P, Sinibaldi E, Caccavaro S, Tortora G, Menciassi A and Dario P (2011) A novel magnetic actuation system for miniature swimming robots. *IEEE Transactions on Robotics* 27: 769–779.

Pan Y, Lin W, Li J, et al. (2009) Reduced efficiency of magnetotaxis in magnetotactic coccoid bacteria in higher than geomagnetic fields. *Biophysical Journal* 97: 986–991.

Ou Y, Kim DH, Kim P, Kim MJ and Julius AA (2012) Motion control of magnetized *Tetrahymena pyriformis* cells by magnetic field with model predictive control. *The International Journal of Robotics Research* 31: 1–11.

Yang C, Chen C, Ma Q, Wu L and Song Y (2012) Dynamic model and motion mechanism of magnetotactic bacteria with two lateral flagellar bundles. *Journal of Bionic Engineering* 9: 200–210.

Zhang L, Abbott JJ, Dong L, Kratochvil BE, Bell D and Nelson BJ (2009) Artificial bacterial flagella: fabrication and magnetic control. *Applied Physics Letters* 94: 4107.